On A Nascent Mathematical-Physical Latency-Information Theory, Part I: The Revelation Of Powerful And Fast Knowledge-Unaided Power-Centroid Radar

Erlan H. Feria
Department of Engineering Science and Physics
The College of Staten Island of the City University of New York
E-mail feria@mail.csi.cuny.edu Web site http://feria.csi.cuny.edu

ABSTRACT

In this first part of the latest latency-information theory (LIT) and applications paper series powerful and fast 'knowledge-unaided' power-centroid (F-KUPC) radar is revealed. More specifically, it is found that for real-world airborne moving target indicator radar subjected to severely taxing environmental conditions F-KUPC radar approximates the signal to interference plus noise ratio (SINR) radar performance derived with more complex knowledge-aided power-centroid (KAPC) radar. KAPC radar was discovered earlier as part of DARPA's 2001-2005 knowledge-aided sensor signal processing expert reasoning (KASSPER) Program and outperforms standard prior-knowledge radar schemes by several orders of magnitude in both the compression of sourced intelligence-space of prior-knowledge, in the form of SAR imagery, and the compression of processing intelligence-time of the associated clutter covariance processor, while also yielding an average SINR radar performance that is approximately 1dB away from the optimum. In this paper, it is shown that the average SINR performance of significantly simpler F-KUPC radar emulates that of KAPC radar and, like KAPC radar, outperforms a conventional knowledge-unaided sample covariance matrix inverse radar algorithm by several dBs. The matlab simulation programs that were used to derive these results will become available in the author's Web site.

Index Terms— *Latency, Information, Intel-Space Compression, Intel-Time Compression, Knowledge-Aided, Knowledge-Unaided, Adaptive Radar, Sample Covariance Matrix Inverse*

1. INTRODUCTION

A straight forward approach to adaptive airborne moving target indicator (AMTI) radar, see Fig. 1, that does not use clutter prior-knowledge is the sample covariance matrix inversion (SCMI) scheme that is used to approximate the optimum Wiener-Hopf weighting vector that arises from maximizing target signal to interference plus noise ratio (SINR) for an investigated range-bin [1]. The construction of the optimum Wiener-Hopf algorithm requires knowledge of the interference plus noise covariance of the range-bin. The inverted range-bin interference plus noise covariance is then multiplied by the steering vector of the assumed target to yield a complex weighting vector of dimension NM where N is the number of antenna elements and M is the number of its transmitted pulses during a coherent pulse interval (CPI). This weighting vector is then multiplied by an NM dimensional complex vector that is measured by the radar receiver and reflects range-bin target, clutter and additional radar interferences and noise. The result of this multiplication is a complex scalar variable that is used by the AMTI to determine if a target appears on the range-bin or not. Since the actual interference plus noise covariance is not available in a real-world scenario, the SCMI scheme addresses this issue by using one or more measurements from range-bins that are adjacent to the range-bin in question to construct a sample covariance matrix (SCM). Unfortunately, however, in a real-world non-stationary environment this very simple scheme only crudely approximates the exact range-bin covariance, which often manifests itself in an unsatisfactory SINR radar performance. To address this problem clutter prior-knowledge in the form of SAR imagery has been advanced, such as was done by DARPA in its 2001-2005 knowledge-aided sensor signal processing expert reasoning (KASSPER) Program [2]. The use of these SAR images as prior-knowledge achieves SINR performances that significantly outperform the SCMI algorithm as well as approximate the optimum results derived from the optimum Wiener-Hopf scheme. On the down side, unfortunately, the use of SAR imagery prior-knowledge has the drawback of increasing the complexity of the

This work was supported in part by the Defense Advanced Research Projects Agency (DARPA) under Grant No. FA8750-04-1-004 and the PSC-CUNY Research Awards PSCREG-37-913, 38-247, 39-834, 40-1013

Mobile Multimedia/Image Processing, Security, and Applications 2009, edited by Sos S. Agaian, Sabah A. Jassim,
Proc. of SPIE Vol. 7351, 73510U · © 2009 SPIE · CCC code: 0277-786X/09/$18 · doi: 10.1117/12.819040

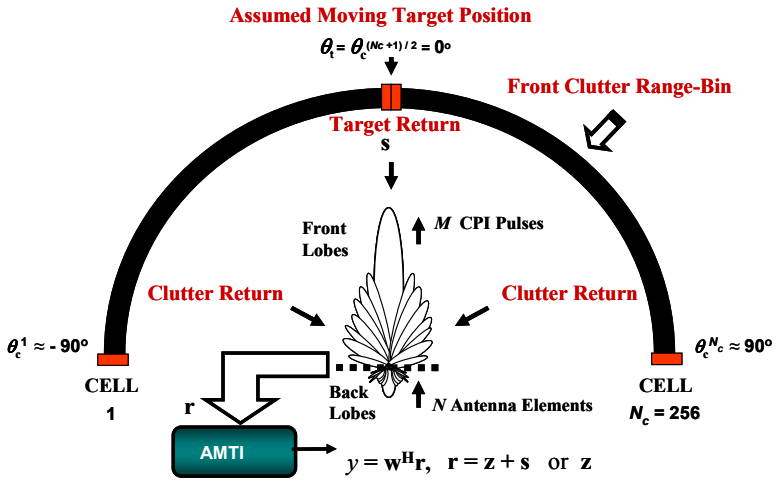

Fig. 1 Airborne Moving Target Indicator Radar System

radar system due to the storage space needs for the 'sourced intelligence-space (or intel-space in short)', i.e. the SAR imagery, and the 'processing intelligence time (or intel-time in short)' needs for the on-line evaluation of the clutter covariance from SAR imagery. To address this problem a novel latency-information theory (LIT) methodology has been advanced [3] whose catalyst was a DARPA KASSPER grant [4] for the compression of SAR imagery via minimum mean squared error (MMSE) predictive-transform (PT) source coding [5], as well as previous Ph.D. work in control theory [6]. In particular, the advanced control work formulated a fundamental parallel processing approach to quantized control using as motivation the discovery in 1978 of an uncertainty-communication/certainty-control duality, unexplored until then, that exists between an uncertainty 'digital' communication problem, i.e. Matched Filters, and a certainty 'quantized' control problem, given the name Matched-Processors from a duality perspective. Thus not surprisingly LIT was formulated by the author as a unified approach to the compression of intel-space—in binary digit or bit units of a passing of time uncertainty nature—and the compression of intel-time—in binary operator or bor units of a configuration of space certainty nature. Using this novel LIT conceptualization a knowledge-aided power-centroid (KAPC) radar algorithm was found that yielded orders of magnitude improvements in both intel-space and intel-time savings over standard techniques. The fundamental idea behind this low storage and very fast clutter prior-knowledge scheme was the use of off-line designed predicted clutter covariances (PCCs). The PCCs were developed using a mathematical model of the physically produced antenna pattern that pointed in the direction of the range-bin power-centroid rather than the target. The objective of this model was to serve as a compensating antenna pattern (CAP) for the information lost from SAR images that had been compressed by a factor of 8,172 in a highly lossy manner. The intel-space compression of these images was also done using a radar blind scheme that made it possible for their use in any type of radar system. The main purpose of this paper, is to show that in fact the aforementioned powerful and fast KAPC scheme can be replaced with an even more powerful and fast 'knowledge-unaided' power-centroid (F-KUPC) scheme. The main virtue of F-KUPC radar is that it does not need the use of clutter prior-knowledge in the form of SAR imagery for its evaluation of the range-bin power-centroid as can be easily verified using matlab simulations of standard radar systems. This is the case since with a very small number of on-line scannings of each range-bin in question a very simple on-line algorithm can be used yielding an outstanding on-line estimation of the prerequisite power-centroid.

The rest of the paper is organized as follows. In Section 2 the optimum AMTI radar defining equations are stated. In Section 3 the sample covariance matrix inverse scheme is summarized. In Section 4 the previously offered KAPC radar algorithm is summarized. In Section 5 the newly revealed F-KUPC radar scheme is advanced. In Section 6 simulations for real-world AMTI radar under severe environmental disturbances are given and then conclusions are drawn.

2. OPTIMUM AIRBORNE MOVING TARGET INDICATOR RADAR

The main defining equations for AMTI radar are summarized next for ease of reference.

2.1 The AMTI Radar System

In Fig. 1 the AMTI radar system is displayed. It consists of: a) N antenna elements that emit M pulses during a coherent pulse interval (*CPI*); b) an antenna pattern with its mainbeam pointing to the assumed target location; and c) a front clutter range-bin mathematically modeled as N_C clutter patches or cells that radiate to the AMTI receiving antenna reflections of the M pulses transmitted by the antenna elements as well as the investigated target steering vector times its power. In our simulations the target power times its steering vector will be normalized to one and the target boresight angle θ_t with respect to the moving AMTI antenna is of zero degrees, i.e. $\theta_t = 0^0$. In addition, the assumed N_C number of cells is even where the boundary line between cells $N_C/2$ and $(N_C+2)/2$ is investigated to determine if a moving target appears there. When N_C has a large value the first and last clutter cells have a clutter boresight angle θ_C^i that is slightly greater than -90^o for $i=1$ and slightly less than 90^o for $i=N_C$, respectively. In Table 1 the N_C, N and M values used in our simulations are summarized along with other radar parameters.

2.2 The Analytical Antenna Pattern Model

Regarding the antenna pattern of Fig. 1, it is assumed that the i^{th} clutter cell receives from this pattern the i^{th} antenna gain which is derived from the following analytical expression

$$g_i(\theta_t) = K^f \left| \frac{\sin\left\{ N\pi \frac{d}{\lambda}(\sin(\theta_C^i) - \sin(\theta_t)) \right\}}{\sin\left\{ \pi \frac{d}{\lambda}(\sin(\theta_C^i) - \sin(\theta_t)) \right\}} \right|^2 / N^2 \tag{1}$$

where $i=1,..,N_C$, θ_t is the target boresight angle, d is the antenna inter-element spacing, λ is the operating-wavelength, and K^f is the front antenna gain constant.

2.3 The AMTI Scalar Complex Output

The scalar complex output of the AMTI system is given by the expression

$$y = \mathbf{w}^H(\mathbf{z}+\mathbf{s}) \tag{2}$$

where: a) **s** is an NM dimensional complex normalized steering vector representing the target; b) **z** is an NM dimensional complex interference plus noise complex vector; c) 'H' denotes transpose and complex conjugation; and d) **w** is an NM dimensional complex weighting vector that is designed with the view of maximizing SINR.

2.4 The Signal to Interference Plus Noise Ratio (SINR)

The SINR expression that is maximized is given by

$$\text{SINR}=\mathbf{w}^H\mathbf{s}\mathbf{s}^H\mathbf{w}/\ \mathbf{w}^H\text{C}\mathbf{w}. \tag{3}$$

where $\mathbf{w}^H\mathbf{s}\mathbf{s}^H\mathbf{w}$ is the signal power in (2) and $\mathbf{w}^H\text{C}\mathbf{w}$ is the interference plus noise power in (2) with C being the covariance of the interference plus noise, i.e. $\text{C}=\text{E}[\mathbf{z}^H\mathbf{z}]$.

2.5 The Target Steering Vector s

The normalized steering vector for the target is given by the expressions

$$\mathbf{s} = [\underline{\mathbf{s}}_1(\theta_t)\ \ \underline{\mathbf{s}}_2(\theta_t) \ldots . \underline{\mathbf{s}}_M(\theta_t)]^T / \sqrt{NM} \tag{4}$$

$$\underline{\mathbf{s}}_k(\theta_t) = e^{j2\pi(k-1)\overline{f}_D^t}\, \underline{\mathbf{s}}_1(\theta_t) \quad for\ k = 1,\ldots,M \tag{5}$$

$$\underline{\mathrm{s}}_1(\theta_t) = [\mathrm{s}_{1,1}(\theta_t)\ \ \mathrm{s}_{2,1}(\theta_t)\ \ \ldots .\ \ \mathrm{s}_{\mathrm{N},1}(\theta_t)] \tag{6}$$

$$s_{k,1}(\theta_t) = e^{j2\pi(k-1)\bar{\theta}_t} \;\; for\; k = 1,\ldots,N \tag{7}$$

$$\bar{f}^{t}_{D} = f^{t}_{D} / f_r \tag{8}$$

$$f^{t}_{D} = 2v_p / \lambda = 2(v_p / c) f_c \tag{9}$$

$$f_r = 1/T_r \tag{10}$$

$$\bar{\theta}_t = (d/\lambda)\sin(\theta_t) \tag{11}$$

where: a) θ_t is the boresight position of the target which is of 0° for the case displayed in Fig. 1 as well as in the simulations; b) f_c is the carrier (or operating) frequency; c) $\bar{\theta}_t$ is the normalized θ_t; d) T_r is the pulse repetition interval (PRI); e) f_r is the pulse repetition frequency (PRF); f) v_p is the target radial velocity; g) c is the speed of light; h) f^{t}_{D} is the target Doppler; and i) $\bar{f}^{t}_{D}$ is the normalized Doppler.

2.6 The Interference Plus Noise Covariance C=E[$\mathbf{z}^H\mathbf{z}$]

The interference plus noise covariance C is given by the following covariance matrix tapers (CMTs) structure [7]

$$\mathrm{C} = \{ (\mathrm{C}^{f}_{c} + \mathrm{C}^{b}_{c}) \,\mathrm{O}\, (\mathrm{C}_{\mathrm{RW}} + \mathrm{C}_{\mathrm{ICM}} + \mathrm{C}_{\mathrm{CM}})\} + \{\mathrm{C}_{\mathrm{J}} \,\mathrm{O}\, \mathrm{C}_{\mathrm{CM}}\} + \mathrm{C}_{\mathrm{n}} \tag{12}$$

where $\mathbf{C}_{\mathrm{n}}$, C^{f}_{c}, C^{b}_{c}, $\mathbf{C}_{\mathrm{J}}$, $\mathbf{C}_{\mathrm{RW}}$, $\mathbf{C}_{\mathrm{ICM}}$ and $\mathbf{C}_{\mathrm{CM}}$ are covariance matrices of dimension *NM x NM* and the symbol 'O' denotes a Hadamard product or element by element multiplication. These covariances correspond to: $\mathbf{C}_{\mathrm{n}}$ to thermal white noise; C^{f}_{c} to front clutter; C^{b}_{c} to back clutter; $\mathbf{C}_{\mathrm{J}}$ to jammer; $\mathbf{C}_{\mathrm{RW}}$ to range walk; $\mathbf{C}_{\mathrm{ICM}}$ to internal clutter motion; and $\mathbf{C}_{\mathrm{CM}}$ to channel mismatch. The defining expressions for each of these covariances are given next starting with the front clutter covariance C^{f}_{c} which in knowledge-aided radar is evaluated making use of prior-knowledge such as SAR imagery (2). Note that the back clutter covariance C^{b}_{c} will be assumed to offer a negligible contribution to C since we will be assuming in our simulations that the back antenna gain constant K^b is of 10^{-4}, i.e. – 40 dBs.

2.6.1 The Front Clutter Covariance C^{f}_{c}

$$\mathrm{C}^{f}_{c} = \sum_{i=1}^{N_C} x_i \mathrm{g}_i(\theta_t)\mathbf{c}_i(\theta_{AAM})\mathbf{c}_i^H(\theta_{AAM}) \tag{13}$$

$$\mathbf{c}_i(\theta_{AAM}) = [{}_f\underline{\mathbf{c}}_1(\theta^i_c,\theta_{AAM}) \;\; {}_f\underline{\mathbf{c}}_2(\theta^i_c,\theta_{AAM}) \cdots {}_f\underline{\mathbf{c}}_M(\theta^i_c,\theta_{AAM})]^T \tag{14}$$

$${}_f\underline{\mathbf{c}}_k(\theta^i_c,\theta_{AAM}) = e^{j2\pi(k-1)\bar{f}^{c_f}_{D}(\theta^i_c,\theta_{AAM})}\underline{\mathbf{c}}_1(\theta^i_c) \;\; for\; k = 1,\ldots,M \tag{15}$$

$$\underline{\mathbf{c}}_1(\theta^i_c) = [\mathbf{c}_{1,1}(\theta^i_c) \;\; \mathbf{c}_{2,1}(\theta^i_c) \;\; \ldots. \;\; \mathbf{c}_{\mathrm{N},1}(\theta^i_c)] \tag{16}$$

$$\mathbf{c}_{k,1}(\theta^i_c) = e^{j2\pi(k-1)\bar{\theta}^i_c} \;\; for\; k = 1,\ldots,N \tag{17}$$

$$\bar{f}^{c_f}_{D}(\theta^i_c,\theta_{AAM}) = \beta\bar{\theta}^i_c \tag{18}$$

$$\beta = (v_p T_r)/(d/2) \tag{19}$$

$$\bar{\theta}^i_C = (d/\lambda)\sin(\theta^i_C + \theta_{AAM}) \tag{20}$$

where: a) the index *i* refers to the i^{th} front clutter cell on the front range bin section shown in Fig. 1; b) θ^i_c is the boresight angle of the i^{th} clutter cell; c) θ_{AAM} is the antenna array misalignment angle; d) x_i is the i^{th} front clutter source cell power; e) θ_t is the target boresight angle; f) $g_i(\theta_t)$ is the antenna gain linked to the i^{th} front clutter cell; g) $\mathbf{c}_i(\theta_{AAM})$ is the front *NM* x 1 dimensional and complex i^{th} clutter cell steering vector; h) v_p is the radar platform speed; i) T_r is the PRI; j) f_r is the PRF; k) $\bar{\theta}^i_c$ is the normalized θ^i_c; *l*) *d* is the antenna inter-element spacing; m) λ is the

operating wavelength; and n) β is the ratio of the distance traversed by the radar platform during the PRI, i.e. $v_p T_r$, to the half antenna inter-element spacing, $d/2$. Finally, the first element of the NM by NM matrix C_c^f divided by the noise variance is the front clutter to noise ratio given by

$$\mathrm{CNR}^{\mathrm{f}} = \mathrm{C}_c^f(1,1)/\sigma_n^2 = \sum_{i=1}^{N_c} x_i g_i(\theta_t)/\sigma_n^2 \tag{21}$$

where σ_n^2 is the variance of the thermal white noise whose value is assumed to be of one in our simulations, i.e., σ_n^2=1.

2.6.2. Thermal White Noise Covariance C_n

$$\mathrm{C}_n = \sigma_n^2 I_{NM} \tag{22}$$

where σ_n^2 is the average power of thermal white noise and I_{NM} is an identity matrix of dimension NM by NM.

2.6.3. Jammer Covariance C_J

$$\mathrm{C}_J = \sum_{i=1}^{N_J} p_i g_i(\theta_t)(I_M \otimes 1_{N\times N}) \mathrm{O} (\mathrm{j}(\theta_J^i) \bullet \mathrm{j}(\theta_J^i)^H) \tag{23}$$

$$\mathbf{j}(\theta_J^i) = [\mathbf{j}_1(\theta_J^i)\ \ \mathbf{j}_2(\theta_J^i) \ldots \mathbf{j}_M(\theta_J^i)]^T \tag{24}$$

$$\mathbf{j}_k(\theta_J^i) = \mathbf{j}_1(\theta_J^i) \quad for\ k = 1,\ldots,M \tag{25}$$

$$\mathbf{j}_1(\theta_J^i) = [\mathrm{j}_{1,1}(\theta_J^i)\ \ \mathrm{j}_{2,1}(\theta_J^i)\ \ldots\ \mathrm{j}_{N,1}(\theta_J^i)] \tag{26}$$

$$j_{k,1}(\theta_J^i) = e^{j2\pi(k-1)\bar{\theta}_J^i} \quad for\ k = 1,\ldots,N \tag{27}$$

$$\bar{\theta}_J^i = \frac{d}{\lambda}\sin(\theta_J^i) \tag{28}$$

where: a) the index i refers to the i^{th} jammer on the range bin; b) N_J is the total number of jammers; c) θ_J^i is the boresight angle of the i^{th} jammer ; d) $\otimes$ is the Kronecker (or tensor) product; e) I_M is an identity matrix of dimension M by M; f) 1_{NxN} is a unity matrix of dimension N by N; g) p_i is the i^{th} jammer power; and h) $\mathbf{j}(\theta_J^i)$ is the NM x 1 dimensional and complex i^{th} jammer steering vector that is noted from (23)-(28) to be Doppler independent.

The first element of the NM by NM matrix C_J defines the jammer to noise ratio

$$\mathrm{JNR} = \mathrm{C}_J(1,1)/\sigma_n^2 = \sum_{i=1}^{N_J} p_i g_i(\theta_t)/\sigma_n^2 \tag{29}$$

2.6.4. Range Walk Covariance CMT C_{RW}

$$\mathrm{C}_{RW} = \mathrm{C}_{RW}^{time} \otimes \mathrm{C}_{RW}^{space} \tag{30}$$

$$[\mathrm{C}_{RW}^{time}]_{i,k} = \rho^{|\mathrm{i-k}|} \tag{31}$$

$$\mathrm{C}_{RW}^{space} = 1_{NxN} \tag{32}$$

$$\rho = \Delta A / A = \Delta A / \{\Delta R \Delta\theta\} = \Delta A / \{(c/B)\Delta\theta\} \tag{33}$$

where: a) c is the velocity of light; b) B is the bandwidth of the compressed pulse; c) ΔR is the range-bin radial width; d) $\Delta\theta$ is the mainbeam width; e) A is the area of coverage on the range bin associated with $\Delta\theta$ at the beginning of the range walk; f) ΔA is the remnants of area A after the range bin migrates during a CPI; and g) ρ is the fractional part of A that remains after the range walk.

2.6.5. Internal Clutter Motion Covariance CMT C_{ICM}

$$\mathrm{C}_{ICM} = \mathrm{C}_{ICM}^{time} \otimes \mathrm{C}_{ICM}^{space} \tag{34}$$

$$[\mathbf{C}_{ICM}^{time}]_{i,k} = \frac{r}{r+1} + \frac{1}{r+1}\frac{(b\lambda)^2}{(b\lambda)^2 + (4\pi\,|\,k\text{-}i\,|\,T_r)^2} \tag{35}$$

$$\mathrm{C}_{ICM}^{space} = 1_{NxN} \tag{36}$$

$$10\log_{10} r = -15.5\log_{10}\omega - 12.1\log_{10} f_c + 63.2 \tag{37}$$

where: a) f_c is the carrier frequency in megahertz; b) ω is the wind speed in miles per hour; c) r is the ratio between the dc and ac terms of the clutter Doppler power spectral density; d) b is a shape factor that has been tabulated; e) c is the speed of light; and f) T_r is the pulse repetition interval.

2.6.6. Channel Mismatch Covariance CMT C_{CM}

$$\mathrm{C}_{CM} = \mathrm{C}_{NB} \,\mathrm{o}\, \mathrm{C}_{FB} \,\mathrm{o}\, \mathrm{C}_{AD} \tag{38}$$

where C_{NB}, C_{FB} and C_{AD} are composite *CMT*s that are defined next.

2.6.7. Finite Bandwidth: C_{FB} is a finite (nonzero) bandwidth (FB) channel mismatch CMT

$$\mathrm{C}_{FB} = \mathrm{C}_{FB}^{time} \otimes \mathrm{C}_{FB}^{space} \tag{39}$$

$$\mathrm{C}_{FB}^{time} = 1_{MxM} \tag{40}$$

$$[\mathrm{C}_{FB}^{space}]_{i,k} = (1-\Delta\varepsilon/2)^2 \sin\mathrm{c}^2(\Delta\phi/2) \quad for \quad i \neq k \tag{41}$$

$$[\mathrm{C}_{FB}^{space}]_{i,i} = 1 - \Delta\varepsilon + \frac{1}{3}\Delta\varepsilon^2 \quad for \quad i = 1,..,N \tag{42}$$

where $\Delta\varepsilon$ and $\Delta\phi$ denote the peak deviations of decorrelating random amplitude and phase channel mismatch, respectively. The square term in (42) corrects an error in the derivation of equation (4.21) in [7].

2.6.8. Angle Dependent: C_{AD} is a reasonably approximate angle-independent CMT for angle-dependent (AD) channel mismatch [7] given by

$$\mathrm{C}_{AD} = \mathrm{C}_{AD}^{time} \otimes \mathrm{C}_{AD}^{space} \tag{43}$$

$$\mathrm{C}_{AD}^{time} = 1_{MxM} \tag{44}$$

$$[\mathrm{C}_{AD}^{space}]_{i,k} = \mathrm{sinc}(B\left|k-i\right|\frac{\mathrm{d}}{\lambda f_\mathrm{c}}\sin(\Delta\theta)) \; for \;\; i \neq k \tag{45}$$

$$[\mathrm{C}_{AD}^{space}]_{i,i} = 1 \tag{46}$$

where B is the bandwidth of an ideal bandpass filter and $\Delta\theta$ is a suitable measure of mainbeam width.

2.6.9. Angle Independent Narrowband: C_{NB} is an angle-independent narrowband or NB channel mismatch CMT

$$\mathrm{C}_{NB} = \mathbf{q}\mathbf{q}^H \tag{47}$$

$$\mathrm{q} = \left[\underline{\mathrm{q}}_1 \; \underline{\mathrm{q}}_2 \cdots \underline{\mathrm{q}}_M\right]^T \tag{48}$$

$$\underline{\mathrm{q}}_k = \underline{\mathrm{q}}_1 \quad for\; k = 1,..,M \tag{49}$$

$$\underline{\mathrm{q}}_1 = \left[\varepsilon_1 e^{j\gamma_1} \;\; \varepsilon_2 e^{j\gamma_2} \;\; \ldots \;\; \varepsilon_N e^{j\gamma_N}\right] \tag{50}$$

where $\Delta\varepsilon_1,\ldots,\Delta\varepsilon_N$ and $\Delta\gamma_1,\ldots,\Delta\gamma_N$ denote amplitude and phase errors, respectively.

2.7 The Weighing Vector w

The weighting vector **w** that maximizes the SINR (3) is derived via the use of Schwarz's inequality which yields the Wiener-Hopf equation

$$\mathbf{w} = \mathrm{C}^{-1}\mathbf{s} \tag{51}$$

where C is the interference plus noise covariance (12) and **s** is the normalized steering vector of the target.

2.8 The Optimum SINR Performance

The optimum SINR performance, $\mathrm{SINR}_{\mathrm{Opt}}$, is derived from the substitution of the weighting vector (51) in (3) to yield

$$\mathrm{SINR}_{\mathrm{Opt}} = \mathbf{s}^{\mathrm{H}}\mathrm{C}^{-1}\mathbf{s}. \tag{52}$$

3. THE SAMPLE COVARIANCE MATRIX INVERSE

The sample covariance matrix inverse (SCMI) algorithm is stated next.

The SCMI Weighting Vector $\mathbf{w}_{\mathrm{SCMI}}$

The SCMI counterpart of the optimum SINR Wiener-Hopf weighting vector (51) is as follows

$$\mathbf{w}_{\mathrm{SCMI}} = {}^{SCM}\mathrm{C}^{-1}\,\mathbf{s} \tag{53}$$

$${}^{SCM}\mathrm{C} = \frac{1}{L_{SCM}}\sum_{i=1}^{L_{SCM}} \mathbf{Z}_i\mathbf{Z}_i^H + \sigma^2_{diag}\, I \tag{54}$$

where: a) ${}^{SCM}\mathrm{C}$ denotes the sample covariance matrix (SCM); b) $\sigma^2_{diag}I$ is a diagonal loading term where σ^2_{diag} =10 is used in our simulations to address numerical problems linked with the ${}^{SCM}\mathrm{C}$ inversion: and c) $\{\mathbf{Z}_i,\ i=1,..,L_{SCM}\}$ denotes L_{SCM} samples from L_{RB} range-bins. Thus

$$L_{SCM} = L_{Scan}L_{RB} \tag{55}$$

where L_{Scan} represents the number of scans of L_{RB} range-bins. In our simulations we will use L_{SCM} =256 where the number of range bins L_{RB} is 64 range-bins for a 1024 by 256 SAR image to be discussed in Section 6 and the number of scans L_{Scan} of this image will be 4.

3.2 The Simulation Scheme

To derive the set of range-bin measurements $\{\mathbf{Z}_i,\ i=1,..,L_{SCM}\}$ the following simulation algorithm will be used

$$\mathbf{Z}_i = \mathrm{C}_i^{1/2}\mathbf{n}_i \tag{56}$$

where $\mathbf{n}_i$ is a zero mean, unity variance, NM dimensional complex random draw and C_i is the interference plus noise covariance (12) associated with the i^{th} range-bin. All the radar and environmental conditions that are used to evaluate expression (12) for each range-bin are summarized in Table 1, inclusive of jammer assumptions.

4. THE KNOWLEDGE-AIDED POWER-CENTROID ALGORITHM

In this section the knowledge-aided power-centroid (KAPC) algorithm is stated which derives the prerequisite range-bin power-centroid from the stored SAR imagery.

4.1 The Knowledge-Aided Power-Centroid (KAPC) Algorithm

The knowledge-aided power-centroid (KAPC) algorithm is given by the following weighting vector expressions

$$\mathbf{w}_{KAPC} = [{}^{KAPC}\mathrm{C}]^{-1}\mathbf{s} \tag{57}$$

$${}^{KAPC}\mathrm{C} = \{\,(\,{}^{KAPC}\mathrm{C}_{\mathrm{c}}^{\mathrm{f}} + \mathrm{C}_{\mathrm{c}}^{\mathrm{b}}\,)\ \mathrm{O}\ (\mathrm{C}_{\mathrm{RW}} + \mathrm{C}_{\mathrm{ICM}} + \mathrm{C}_{\mathrm{CM}})\} + \{\mathrm{C}_{\mathrm{J}}\,\mathrm{O}\,\mathrm{C}_{\mathrm{CM}}\} + \mathrm{C}_{\mathrm{n}} \tag{58}$$

where the covariances C_c^b, $\mathbf{C}_{RW}$, $\mathbf{C}_{ICM}$, $\mathbf{C}_{CM}$, $\mathbf{C}_J$, and $\mathbf{C}_n$ are the same as those for the interference plus noise covariance $\mathbf{C}$ given by expression (12), and ${}^{KAPC}C_c^f$ predicts C_c^f of (12).

4.1.1 The *KAPC* Predicted Front Clutter Cell Covariance ${}^{KAPC}C_c^f$

The defining expressions for ${}^{KAPC}C_c^f$ are given by

$$ {}^{KAPC}C_c^f = \sum_{i=1}^{N_C} \bar{g}_i(\theta_C^{\mathbf{C(xOg)}})\mathbf{c}_i(\theta_{AAM})\mathbf{c}_i^H(\theta_{AAM}) \tag{59} $$

$$ \mathbf{C(xOg)} = \sum_{i=1}^{N_C} i x_i g_i(\theta_t) / \sum_{i=1}^{N_C} x_i g_i(\theta_t) \tag{60} $$

$$ \theta_C^{\mathbf{C(xOg)}} = \mathbf{C(xOg)}\pi / N_C \text{ - } \pi/2 \tag{61} $$

$$ \mathbf{xOg} = [x_1 g_1 \;\; x_2 g_2 \;\; .... \;\; x_{N_C} g_{N_C}] \tag{62} $$

where: a) $\mathbf{c}_i(\theta_{AAM})$, x_i and $g_i(\theta_t)$ are as defined for C_c^f (13); b) $\mathbf{xOg}$ is the Hadamard product or element by element product of the power emitted by the investigated range-bin $\mathbf{x} = [x_1 \;\; x_2 \;\; .... \;\; x_{N_C}]$ and the front antenna gain $\mathbf{g} = [g_1 \;\; g_2 \;\; .... \;\; g_{N_C}]$; c) $\mathbf{C(xOg)}$ is the power-centroid which can be any real number from 1 to N_C; d) $\theta_C^{\mathbf{C(xOg)}}$ is the power-centroid boresight angle in radians; and e) $\bar{g}_i(\theta_C^{\mathbf{C(xOg)}})$ is an appropriately normalized antenna pattern version of (1) that is shifted to the power-centroid and serves as a compensating antenna pattern (CAP) for the lack of either partial or total prior knowledge about the clutter.

4.1.2 The Compensating Antenna Pattern $\bar{g}_i(\theta_C^{\mathbf{C(xOg)}})$

The CAP predicts the clutter-antenna-gain product set $\{x_i g_i(\theta_t) : i = 1,...,N_C\}$ of C_c^f (13) and is defined by the following antenna pattern expression

$$ \bar{g}_i(\theta_C^{\mathbf{C(xOg)}}) = K \left| \frac{\sin\left\{ N\pi \frac{d}{\lambda} (\sin(\theta_C^i) - \sin(\theta_C^{\mathbf{C(xOg)}})) \right\}}{\sin\left\{ \pi \frac{d}{\lambda} (\sin(\theta_C^i) - \sin(\theta_C^{\mathbf{C(xOg)}})) \right\}} \right|^2 \tag{63} $$

$$ {}^{KAPC}C_c^f(1,1) = C_c^f(1,1) \tag{64} $$

where K is a normalizing gain that results in the matching of the average clutter power of the front clutter covariance C_c^f and its prediction ${}^{KAPC}C_c^f$. This scheme which is generally suboptimum since it only approximates the true expression for C_c^f will be found in our simulations to be approximately 1 dB away from the optimum Wiener-Hopf algorithm due to its evaluation of the clutter power-centroid from the true clutter (60) which is available as prior knowledge. However, it must also be noted that earlier in [3]-[4] it had been shown that this scheme also produces outstanding results when the power-centroid of (60) is derived using a SAR image that is a reconstructed version of an original SAR image that is highly lossy compressed.

5. THE KNOWLEDGE-UNAIDED POWER-CENTROID ALGORITHMS

Two power-centroid schemes that do not use clutter prior-knowledge are stated next. The first is a knowledge-unaided power-centroid (KUPC) algorithm that evaluates the power-centroid from the same on-line range-bin measurements $\{\mathbf{Z}_i, i=1,..,L_{SCM}\}$ that are used to construct the SCMI algorithm. This KUPC scheme requires a predicted clutter covariance (PCC) matrix to be derived on-line and has at its disposal full or partial knowledge of other radar interferences and noise covariances. The second scheme is a fast KUPC (F-KUPC) algorithm that quantizes the power-centroid derived from $\{\mathbf{Z}_i, i=1,..,L_{SCM}\}$. The quantized power-centroid is then used to extract from a memory a PCC that had been previously designed off-line using a CAP directed towards the quantized power-centroid.

5.1 The Knowledge-Unaided Power-Centroid (KUPC) Algorithm

The KUPC algorithm is given by the following weighting vector expressions

$$\mathbf{w}_{KUPC} = [{}^{KUPC}\mathrm{C}]^{-1}\mathbf{s} \tag{65}$$

$${}^{KUPC}\mathrm{C} = \{ ({}^{KUPC}\mathrm{C}_{\mathrm{c}}^{\mathrm{f}} + \mathrm{C}_{\mathrm{c}}^{\mathrm{b}}) \, \mathrm{O} \, (\mathrm{C}_{\mathrm{RW}} + \mathrm{C}_{\mathrm{ICM}} + \mathrm{C}_{\mathrm{CM}}) \} + \{ \mathrm{C}_{\mathrm{J}} \, \mathrm{O} \, \mathrm{C}_{\mathrm{CM}} \} + \mathrm{C}_{\mathrm{n}} \tag{66}$$

where the covariances C_c^b, $\mathbf{C}_{\mathrm{RW}}$, $\mathbf{C}_{\mathrm{ICM}}$, $\mathbf{C}_{\mathrm{CM}}$, $\mathbf{C}_{\mathrm{J}}$, and $\mathbf{C}_{\mathrm{n}}$ are the same as those for the interference plus noise covariance $\mathbf{C}$ given by expression (12) and are either assumed to be zero or known, and ${}^{KUPC}\mathrm{C}_{\mathrm{c}}^{\mathrm{f}}$ predicts the front clutter cell covariance for $\mathrm{C}_{\mathrm{c}}^{\mathrm{f}}$ in (12).

5.1.1 The *KUPC* Predicted Front Clutter Cell Covariance ${}^{KUPC}\mathrm{C}_{\mathrm{c}}^{\mathrm{f}}$

The defining expressions for ${}^{KUPC}\mathrm{C}_{\mathrm{c}}^{\mathrm{f}}$ are given by

$${}^{KUPC}\mathrm{C}_{\mathrm{c}}^{\mathrm{f}} = \sum_{i=1}^{N_C} \hat{\mathrm{g}}_i(\theta_C^{\overline{C}}) \mathbf{c}_i(\theta_{AAM}) \mathbf{c}_i^H(\theta_{AAM}) \tag{67}$$

$$\overline{C} = \begin{cases} 1, & \overline{\mathbf{M}} < -\dfrac{N_C - 1}{2} \\ \dfrac{N_C + 1}{2} + \overline{\mathbf{M}}, & -\dfrac{N_C - 1}{2} \le \overline{\mathbf{M}} \le \dfrac{N_C - 1}{2} \\ N_C, & \dfrac{N_C - 1}{2} < \overline{\mathbf{M}} \end{cases} \tag{68}$$

$$\overline{\mathbf{M}} = \sum_{i=2}^{N+M-1} k_{\mathrm{i}} \mathrm{Imag}[m_i] \Big/ m_1 \tag{69}$$

$$\theta_C^{\overline{C}} = \frac{\pi}{N_C} \left(\overline{C} - \frac{N_C + 1}{2} \right) \tag{70}$$

$$-\frac{N_C - 1}{N_C} \frac{\pi}{2} \le \theta_C^{\overline{C}} \le \frac{N_C - 1}{N_C} \frac{\pi}{2} \tag{71}$$

$$\hat{g}_i(\theta_C^{\overline{C}}) = \hat{K} \left| \frac{\sin\left\{ N\pi \dfrac{d}{\lambda} (\sin(\theta_C^i) - \sin(\theta_C^{\overline{C}})) \right\}}{\sin\left\{ \pi \dfrac{d}{\lambda} (\sin(\theta_C^i) - \sin(\theta_C^{\overline{C}})) \right\}} \right|^2 \tag{72}$$

$${}^{KUPC}\mathbf{C}_{\mathrm{c}}^{\mathrm{f}}(1,1) = m_1 \tag{73}$$

where: a) $\mathbf{c}_i(\theta_{AAM})$ is as defined for $\mathrm{C}_{\mathrm{c}}^{\mathrm{f}}$ (13); b) $\overline{C}$ is the estimated power-centroid of the range-bin using the sample covariance matrix in (54), and inclusive of any type of disturbance and noise; c) $\overline{\mathrm{M}}$ is a real scalar quantity which is a function of an appropriately determined set of constants $\{k_i\}$, the real power of the on-line derived measurements $\{\mathbf{Z}_i\}$ or m_1, and the imaginary part or Imag[.] of each element of a set of $N+M-2$ distinct and complex correlations $\{m_i\}$ selected

from the first row of the NM x NM dimensional sample covariance matrix (SCM) in (54), e.g. when M=N=2 the three correlation elements $\{m_i: i=1,2,3\}$ are the first, second, and fourth elements of the SCM's first row as seen below

$$\frac{1}{L_{SCM}}\sum_{i=1}^{L_{SCM}}\mathbf{Z}_i\mathbf{Z}_i^H=\begin{bmatrix} m_1 & m_2 & X & m_3 \\ X & X & X & X \\ X & X & X & X \\ X & X & X & X \end{bmatrix} \tag{74}$$

and when M=N=3 the five correlation elements $\{m_i: i=1,2,3,4,5\}$ are as seen below

$$\frac{1}{L_{SCM}}\sum_{i=1}^{L_{SCM}}\mathbf{Z}_i\mathbf{Z}_i^H=\begin{bmatrix} m_1 & m_2 & m_3 & X & X & m_4 & X & X & m_5 \\ X & X & X & X & X & X & X & X & X \\ X & X & X & X & X & X & X & X & X \\ X & X & X & X & X & X & X & X & X \\ X & X & X & X & X & X & X & X & X \\ X & X & X & X & X & X & X & X & X \\ X & X & X & X & X & X & X & X & X \\ X & X & X & X & X & X & X & X & X \\ X & X & X & X & X & X & X & X & X \end{bmatrix}, \tag{75}$$

and so on for higher dimensions; and d) $\theta_C^{\overline{C}}$ is the boresight angle in radians associated with $\overline{C}$; and d) the values of the constant gains $\{k_i\}$ used in our simulations are found from the following expression

$$k_i=-K_{\overline{\mathbf{M}}}(-1)^i\frac{1}{2^{i-2}} \tag{76}$$

where the value of $K_{\overline{\mathbf{M}}}$ is 60.

5.1.2 Justification for KUPC expressions (68), (69) and (76)

The basic idea behind the power-centroid expressions of (68), (69) and (76) is explained next using the optimum M=N=2 case depicted in Fig. 2 for β= 1 as motivation. This figure shows a clutter range-bin made of N_C=4 clutter cells which are symmetrically spaced with respect to the target that is being investigated at the boresight angle of θ_t =0°. Thus we have that the four clutter cell locations { θ_1, θ_2, θ_3, θ_4} send to the two elements of the receiving antenna the clutter-antenna-gain modulated steering expressions $\left\{\sqrt{x_1g_1}\mathbf{v}_1,\sqrt{x_2g_2}\mathbf{v}_2,\sqrt{x_3g_3}\mathbf{v}_3,\sqrt{x_4g_4}\mathbf{v}_4\right\}$, respectively. Furthermore, the two antenna elements in this example produce during a CPI two different measurements. All of these measurements are represented in Fig. 3 with the matrix

$$\begin{bmatrix} z(s_1,t_1) & z(s_2,t_1) \\ z(s_1,t_2) & z(s_2,t_2) \end{bmatrix} \tag{77}$$

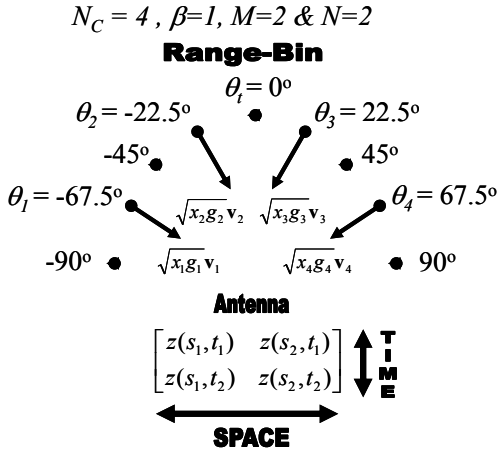

Fig. 2 Space-Time Geometry For An Optimum Power- Centroid Algorithm Example

where the left element of each (s_i,t_j) pair, i.e. s_i, indicates the i^{th} antenna element and the right element t_j denotes the j^{th} received pulse during a CPI, while the four measurement values depicted on the matrix, i.e. $\{z(s_i,t_j)\}$, are a function of the received modulated steering vectors as shown below

$$\mathbf{z} = \begin{bmatrix} z(s_1,t_1) & z(s_1,t_2) & z(s_2,t_1) & z(s_2,t_2) \end{bmatrix}^T = \sum_{i=1}^{4} \sqrt{x_i g_i}\, \mathbf{v}_i \tag{78}$$

with the four clutter steering vectors given by the expression

$$\mathbf{v}_i = \begin{bmatrix} v_i(s_1,t_1) & v_i(s_2,t_1) & v_i(s_1,t_2) & v_i(s_2,t_2) \end{bmatrix}^T = \begin{bmatrix} 1 & e^{j\frac{2\pi d}{\lambda}\sin\theta_i} & e^{j\frac{2\pi d}{\lambda}\sin\theta_i} & e^{j\frac{4\pi d}{\lambda}\sin\theta_i} \end{bmatrix}^T, \quad i=1,2,3,4 \tag{79}$$

Next an expression is found for the correlation matrix $E[\mathbf{x}\mathbf{x}^H]$ under the assumption that each clutter return is uncorrelated from each other, i.e. it is assumed that $E[\sqrt{x_i g_i}\sqrt{x_j g_j}] = 0$ for $i \neq j$ and $E[\sqrt{x_i g_i}\sqrt{x_j g_j}] = x_i g_i$ for $i=j$. Thus it is found via straight forward algebraic manipulations and the symmetry condition $\theta_3 = -\theta_2 = 22.5^o$ and $\theta_4 = -\theta_1 = 67.5^o$ deduced from Fig. 3 that

$$E[\mathbf{x}\mathbf{x}^H] = \begin{bmatrix} \mathbf{M}(t_1,t_1) & \mathbf{M}(t_1,t_2) \\ \mathbf{M}(t_2,t_1) & \mathbf{M}(t_2,t_2) \end{bmatrix} = \begin{bmatrix} \mathbf{M}(t_1,t_1) & \mathbf{M}(t_1,t_2) \\ \mathbf{M}^*(t_1,t_2) & \mathbf{M}(t_1,t_1) \end{bmatrix} \tag{80}$$

$$\mathbf{M}(t_1,t_1) = \begin{bmatrix} m_1 & m_2 \\ m_2^* & m_1 \end{bmatrix}, \qquad \mathbf{M}(t_1,t_2) = \begin{bmatrix} m_2 & m_3 \\ m_1 & m_2 \end{bmatrix} \tag{81}$$

where the three correlation elements in (81) are found from the following three expressions

$$m_1 = x_1 g_1 + x_2 g_2 + x_3 g_3 + x_4 g_4 \tag{82}$$

$$m_2 = x_1 g_1 e^{j\frac{2\pi d}{\lambda}\sin\theta_4} + x_2 g_2 e^{j\frac{2\pi d}{\lambda}\sin\theta_3} + x_3 g_3 e^{-j\frac{2\pi d}{\lambda}\sin\theta_3} + x_4 g_4 e^{-j\frac{2\pi d}{\lambda}\sin\theta_4} \tag{83}$$

and

$$m_3 = x_1 g_1 e^{j\frac{4\pi d}{\lambda}\sin\theta_4} + x_2 g_2 e^{j\frac{4\pi d}{\lambda}\sin\theta_3} + x_3 g_3 e^{-j\frac{4\pi d}{\lambda}\sin\theta_3} + x_4 g_4 e^{-j\frac{4\pi d}{\lambda}\sin\theta_4}. \tag{84}$$

Next the moment expressions (82)-(84) are related to the desired evaluation of C(**xOg**) (60) for the clutter range-bin of Fig. 2 which is for this case as follows:

$$C(\mathbf{xOg}) = \frac{x_1 g_1 .1 + x_2 g_2 .2 + x_3 g_3 .3 + x_4 g_4 .4}{x_1 g_1 + x_2 g_2 + x_3 g_3 + x_4 g_4}. \tag{85}$$

An algebraic manipulation of this expression then yields

$$C(\mathbf{xOg}) = \frac{4+1}{2} + \frac{\begin{bmatrix} 1 & 3 \end{bmatrix}}{2m_1} \begin{bmatrix} x_3 g_3 - x_2 g_2 \\ x_4 g_4 - x_1 g_1 \end{bmatrix}. \tag{86}$$

where the denominator of (85) now appears as m_1 (82) in (86) and the first term to the right of (86) is given by 2.5 which is the assumed boresight position of the target of 0^o as well as the position of the power-centroid when either a symmetrical condition for the clutter, i.e. $x_3 g_3 = x_2 g_2$ and $x_4 g_4 = x_1 g_1$ exits or the clutter difference closest to the target, i.e. $x_3 g_3 - x_2 g_2$, is equal to the negative of three times the clutter difference away form the target, i.e. $-3(x_4 g_4 - x_1 g_1)$. We next use expressions (82)-(84) to derive the following relationships between the real and imaginary parts of m_2 and m_3

$$\begin{bmatrix} \mathrm{Real}[m_1] \\ \mathrm{Real}[m_2] \end{bmatrix} = \begin{bmatrix} 1 & 1 \\ \cos\left(\frac{2\pi d}{\lambda}\sin\theta_3\right) & \cos\left(\frac{2\pi d}{\lambda}\sin\theta_4\right) \end{bmatrix} \begin{bmatrix} x_3 g_3 + x_2 g_2 \\ x_4 g_4 + x_1 g_1 \end{bmatrix} \tag{87}$$

$$\begin{bmatrix} \mathrm{Imag}[m_2] \\ \mathrm{Imag}[m_3] \end{bmatrix} = -\begin{bmatrix} \sin\left(\frac{2\pi d}{\lambda}\sin\theta_3\right) & \sin\left(\frac{2\pi d}{\lambda}\sin\theta_4\right) \\ \sin\left(\frac{4\pi d}{\lambda}\sin\theta_3\right) & \sin\left(\frac{4\pi d}{\lambda}\sin\theta_4\right) \end{bmatrix} \begin{bmatrix} x_3 g_3 - x_2 g_2 \\ x_4 g_4 - x_1 g_1 \end{bmatrix} \tag{88}$$

Solving the linear system of equations (88) for the clutter differences vector under the constraint that the matrix must be invertible, and then substituting this result in (86) yields the desired optimum expression for the range-bin power-centroid C(**xOg**) in term of the three correlation elements of $E[\mathbf{x}\mathbf{x}^H]$, i.e. m_1, m_2 and m_3, as follows

$$C(\mathbf{xOg}) = \frac{4+1}{2} - \frac{[1 \quad 3]}{2m_1}\begin{bmatrix} \sin\left(\frac{2\pi d}{\lambda}\sin\theta_3\right) & \sin\left(\frac{2\pi d}{\lambda}\sin\theta_4\right) \\ \sin\left(\frac{4\pi d}{\lambda}\sin\theta_3\right) & \sin\left(\frac{4\pi d}{\lambda}\sin\theta_4\right) \end{bmatrix}^{-1}\begin{bmatrix} \text{Imag}[m_2] \\ \text{Imag}[m_3] \end{bmatrix} \tag{89}$$

To get an idea of the values derived for this simple and optimum case we evaluate (89) for the assumed symmetrical conditions of Fig. 2 and under the assumption that d/λ=0.5 (also used in our simulations) to yield

$$C(\mathbf{xOg}) = \frac{5}{2} - [2.10405 \quad -2.17625]\begin{bmatrix} \text{Imag}[m_2] \\ \text{Imag}[m_3] \end{bmatrix} \Big/ m_1 \tag{90}$$

This expression can then be rewritten as follows

$$C(xOg) = \frac{5}{2} + \sum_{i=2}^{3} k_i \text{Imag}[m_i] \Big/ m_1, \quad k_2 = -2.10405(-1)^2 \ \ \& \ k_3 = -2.17625(-1)^3 \tag{91}$$

where a comparison of expressions (68), (69) and (76) with (91) should help explain why the forms for expressions (68), (69) and (76) are being used for the real-world radar problem simulated in this paper. It should also be emphasized that the selected simulation values of N=16, M=16 and N_C=256 do not allow us to generalize (89) to include this case. Moreover even if this was possible it is likely that numerical stability problems will surface when dealing with the inversion of high dimensionality matrices. This is why the simple and well behaved expressions (68), (69) and (76) are used by us.

5.2 The Fast Knowledge-Unaided Power-Centroid Algorithm

The fast KUPC or F-KUPC algorithm is characterized by the following weighting vector expressions

$$\mathbf{w}_{F\text{-}KUPC} = [{}^{F\text{-}KUPC}\mathbf{C}]^{-1}\mathbf{s} \tag{92}$$

$${}^{F\text{-}KUPC}\mathbf{C} = \{ ({}^{F-KUPC}\mathbf{C}_c^{\mathrm{f}} + \mathbf{C}_c^{\mathrm{b}}) \, \mathrm{O} \, (\mathbf{C}_{\mathrm{RW}} + \mathbf{C}_{\mathrm{ICM}} + \mathbf{C}_{\mathrm{CM}}) \} + \{ \mathbf{C}_{\mathrm{J}} \, \mathrm{O} \, \mathbf{C}_{\mathrm{CM}} \} + \mathbf{C}_{\mathrm{n}} \tag{93}$$

where the covariances $\mathbf{C}_c^b$, $\mathbf{C}_{\mathrm{RW}}$, $\mathbf{C}_{\mathrm{ICM}}$, $\mathbf{C}_{\mathrm{CM}}$, $\mathbf{C}_{\mathrm{J}}$, and $\mathbf{C}_{\mathrm{n}}$ are the same as those for the interference plus noise covariance $\mathbf{C}$ given by expression (12), and ${}^{F-KUPC}\mathbf{C}_{\mathrm{c}}^{\mathrm{f}}$ predicts the front clutter cell covariance for $\mathbf{C}_{\mathrm{c}}^{\mathrm{f}}$ in (12).

The defining expressions for ${}^{F-KUPC}\mathbf{C}_{\mathrm{c}}^{\mathrm{f}}$ are similar to those for ${}^{KUPC}\mathbf{C}_{\mathrm{c}}^{\mathrm{f}}$ except that the centroid value derived via (68), (69) and (76) are now quantized. Thus

$${}^{F-KUPC}\mathbf{C}_{\mathrm{c}}^{\mathrm{f}} = \sum_{i=1}^{N_C} \overline{\mathrm{g}}_i(\theta_C^{\hat{C}})\mathbf{c}_i(\theta_{AAM})\mathbf{c}_i^H(\theta_{AAM}) = {}^{KUPC}\mathbf{C}_{\mathrm{c}}^{\mathrm{f}}\big|_{C(\mathbf{xOg})=\hat{C}(\mathbf{xOg})} \tag{94}$$

where the quantized power-centroid $\hat{C}$ is defined as follows:

$$\hat{C} = \min_{\hat{C}_i} \left| \overline{C} - \hat{C}_i \right| \tag{95}$$

$$\hat{C}_i \in \left\{ \frac{N_C - 1}{L}, \frac{2(N_C-1)}{L}, \frac{3(N_C-1)}{L}, \ldots, \frac{(L-1)(N_C-1)}{L} \right\} \tag{96}$$

$$\overline{g}_i(\theta_C^{\hat{C}}) = \hat{K} \left| \frac{\sin\left\{ N\pi \frac{d}{\lambda}(\sin(\theta_C^i) - \sin(\theta_C^{\hat{C}})) \right\}}{\sin\left\{ \pi \frac{d}{\lambda}(\sin(\theta_C^i) - \sin(\theta_C^{\hat{C}})) \right\}} \right|^2 \tag{97}$$

$${}^{F-KUPC}\mathbf{C}_{\mathrm{c}}^{\mathrm{f}}(1,1) = m_1 \tag{98}$$

with L denoting the finite number of CAPs that may be used in (94) to predict the $\mathbf{C}_{\mathrm{c}}^{\mathrm{f}}$, and $\overline{C}$ is the unquantized centroid of (68). Clearly this algorithm lends itself to an extremely fast implementation where sets of L predicted clutter covariances (PCCs) are designed off-line for as many antenna array misalignment angles $\{\theta_{\mathrm{AAM}}\}$ as desired. In our simulations, that we discuss next, we will consider two cases for L (or equivalently the number of CAPs). These cases are L=3 and L=11 where in addition N=M=16 and N_{C}=256, and L_{SCM} =256.

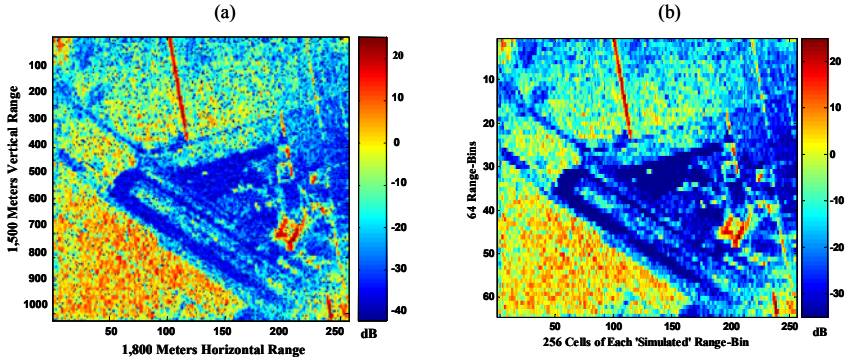

Fig. 3 Synthetic Aperture Radar (SAR) Image of Mojave Airport in California

6. SIMULATION RESULTS

In this section several simulations results are presented that use the 64 by 256 SAR image seen in Fig. 3. The original 4 megabytes SAR image of Fig. 3a is made up of 1,024 by 256 pixel elements representing 1,800 by 1,500 meters of the Mojave Airport in California where each pixel denotes clutter power. Sixteen consecutive rows of Fig. 3a are then averaged to form the 64 x 256 image of Fig. 3b. In our simulation each row of Fig. 3b is a range-bin with 256 clutter cells for each. In addition, the simulation radar parameters, disturbance and noise values used are those of Table 1. The SAR image of Fig. 3 as well as the matlab program used in our simulations will become available in the author's Web site [8] in the near future.

The results are summarized in four figures, i.e. Figs. 4-7. The basic difference between the four figure cases is in the use of jammers and the number of CAPs used. Figs. 4-5 present cases where three jammers are used at boresight angles of -60^{o}, -30^{o} and 45^{o} with corresponding JNR values of 52, 55, and 66 dBs, respectively, while Figs. 6-7 show simulation results with no jammers used. On the other hand, Figs. 4 and 6 present results for eleven CAPs and Figs. 5 and 7 for three CAPs. Each figure case has seven displays. First Figs. 4a, 5a, 6a and 7a show the SINR error in dBs as a function of range-bin where note is made of the average SINR error over all range-bins for the three cases which are the SCMI scheme of (53)-(56), the KAPC scheme of (57)-(64), and the F-KUPC scheme of (92)-(98). For example, in Fig. 4a KAPC is noted to yield an average SINR error of 0.87 dBs, F-KUPC of 1.32 dBs, and SCMI of 7.59 dBs. These results are satisfactory since more than 6 dBs improvements are derived over the SCMI with both the KAPC and F-KUPC schemes, while also yielding in both cases an average SINR radar performance close to the optimum SINR radar performance. In Figs. 4b-7b the power of the KAPC and F-KUPC schemes, i.e. (64) and (98), respectively, is depicted where the fluctuations from range-bin to range-bin found with the F-KUPC case reflects its derivation from the average power m_1 that is derived from the use of the sample covariance matrix (54) without the use of the loading factor of course. In Figs. 4c-7c the range-bin power-centroids corresponding to the KAPC algorithm (60), the KUPC algorithm without centroid quantizations (68), and the F-KUPC algorithm with centroid quantizations (95) are shown. Figs. 4d-g, 5d-g, 6d-g and 7d-g specifically display the radar system performance for range-bin number one. In Figs. 4d-7d the actual range-bin clutter, KAPC predicted clutter power {(59),(63),(64)} and F-KUPC predicted clutter power {(94),(97),(98)} is displayed as a function of clutter cell number. In Fig. 4e-7e the optimum, KAPC, F-KUPC and SCMI SINRs are displayed as a function of normalized Doppler. In Fig. 4f-7f the optimum, KAPC, F-KUPC and SCMI adapted patterns [7] are shown as a function of clutter cell number. Finally in Fig. 4g-7g the optimum, KAPC, F-KUPC and SCMI interference plus noise covariance eigenvalues [7] are plotted for each case.

The results presented in Figs. 4-7 are typical results for the compared schemes as researchers should be able to confirm using their own matlab simulations or those that will become available in [8]. It is thus concluded that F-KUPC radar offers a major improvement over KAPC radar. This result also brings further support to the mathematical uncertainty-information/certainty-latency duality that has resulted in both KAPC and F-KUPC radar. In the second part of this two parts paper series the recently discovered [3] physical dual for our mathematical uncertainty-information/certainty-latency duality is presented in some detail and illustrated with simple physical examples in a more general unification setting.

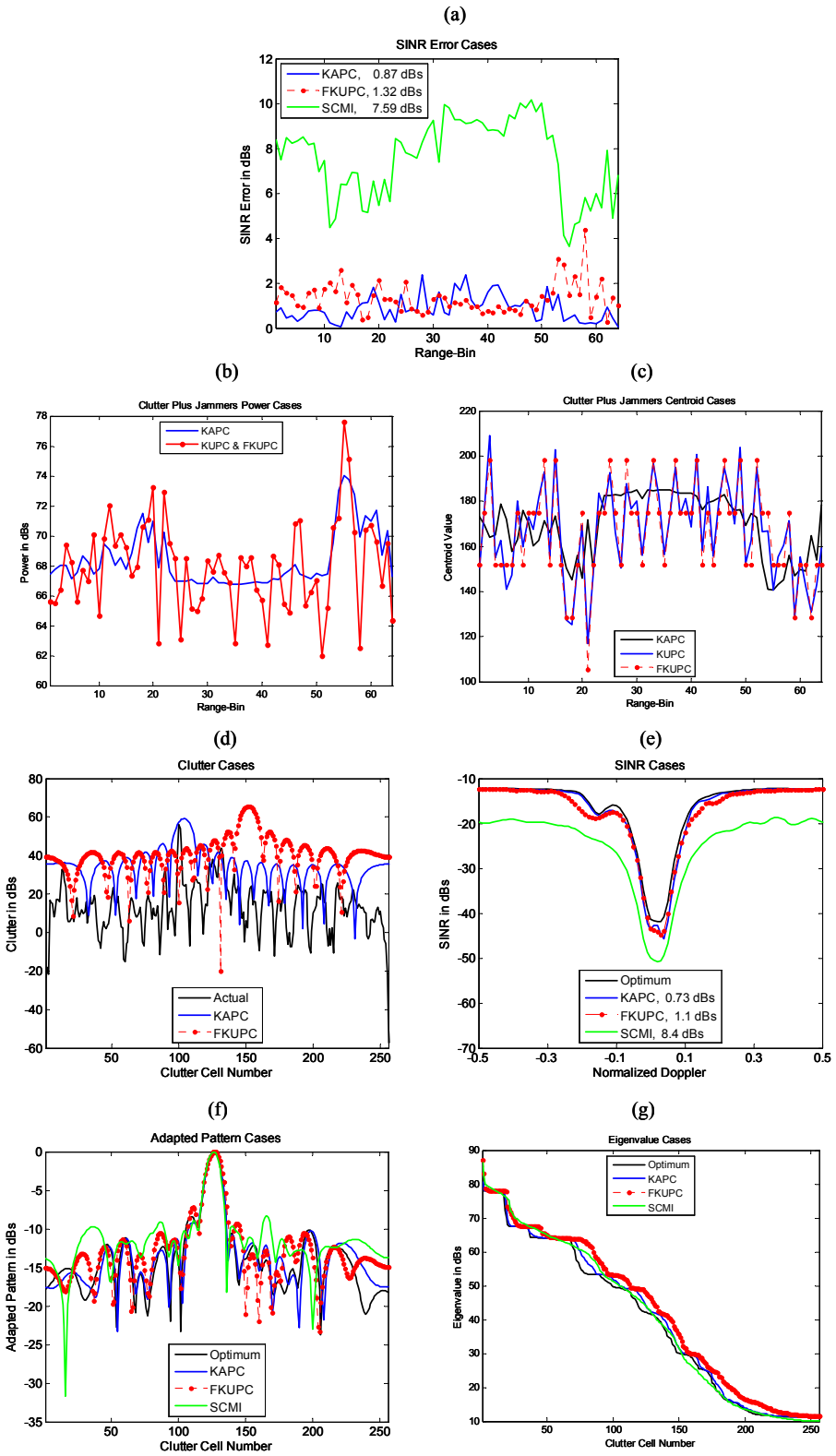

Fig. 4. Eleven (11) CAPs with Jammers at -60°, -30° and 45° with 52, 55, and 66 JNRs in dBs, respectively. (a) SINR Error. (b) Range-Bin Power of Clutter Plus Jammer. (c) Range-Bin Centroid of Clutter Plus Jammer. (d) Range-Bin #1 Clutter and its Predictions. (e) Range-Bin #1 SINRs. (f) Range-Bin #1 Adapted Patterns. (g) Range-Bin #1 Eigenvalues

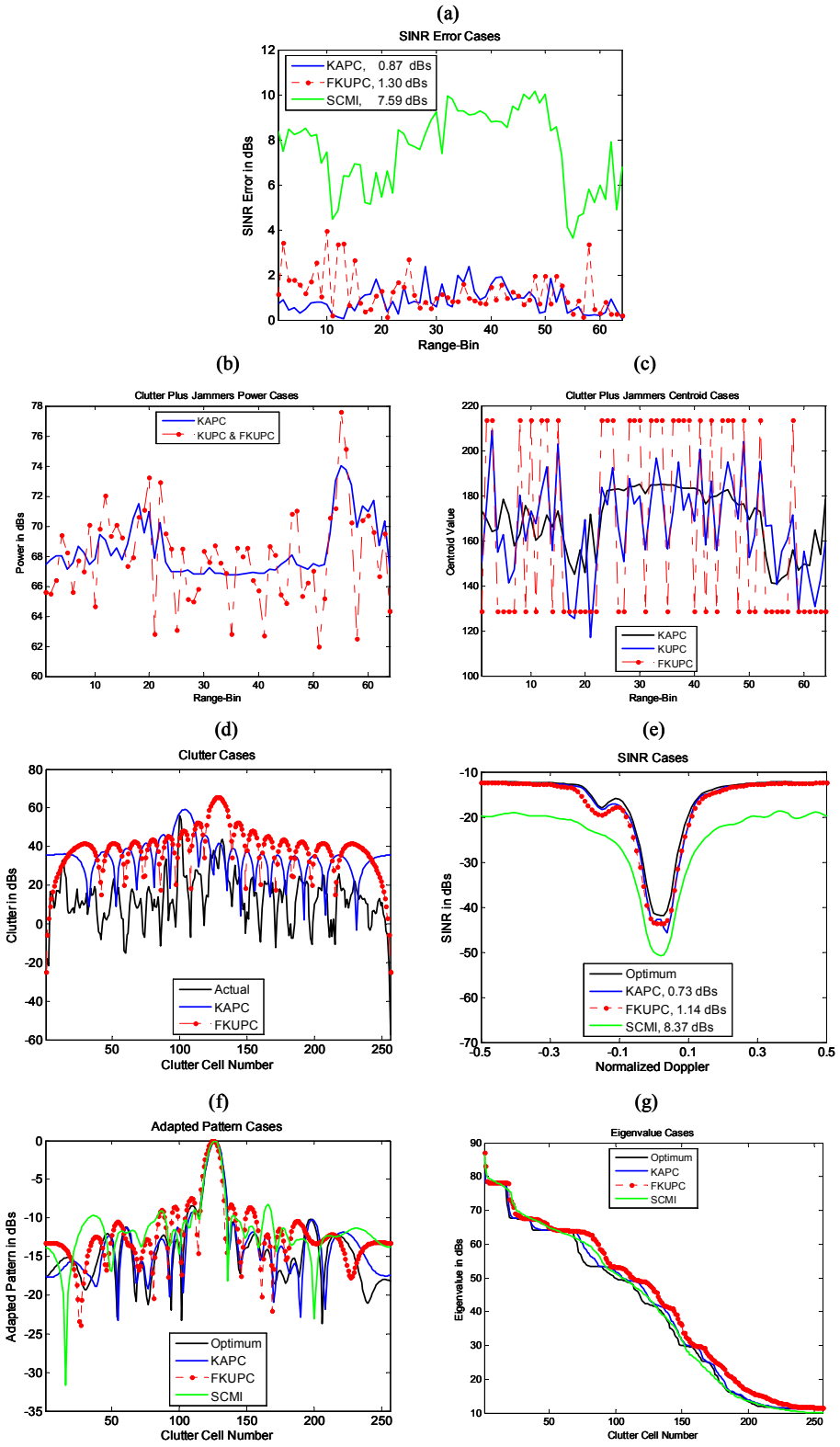

Fig. 5. Three (3) CAPs with Jammers at -60°, -30° and 45° with 52, 55, and 66 JNRs in dBs, respectively. (a) SINR Error. (b) Range-Bin Power of Clutter Plus Jammer. (c) Range-Bin Centroid of Clutter Plus Jammer. (d) Range-Bin #1 Clutter and its Predictions. (e) Range-Bin #1 SINRs. (f) Range-Bin #1 Adapted Patterns. (g) Range-Bin #1 Eigenvalues

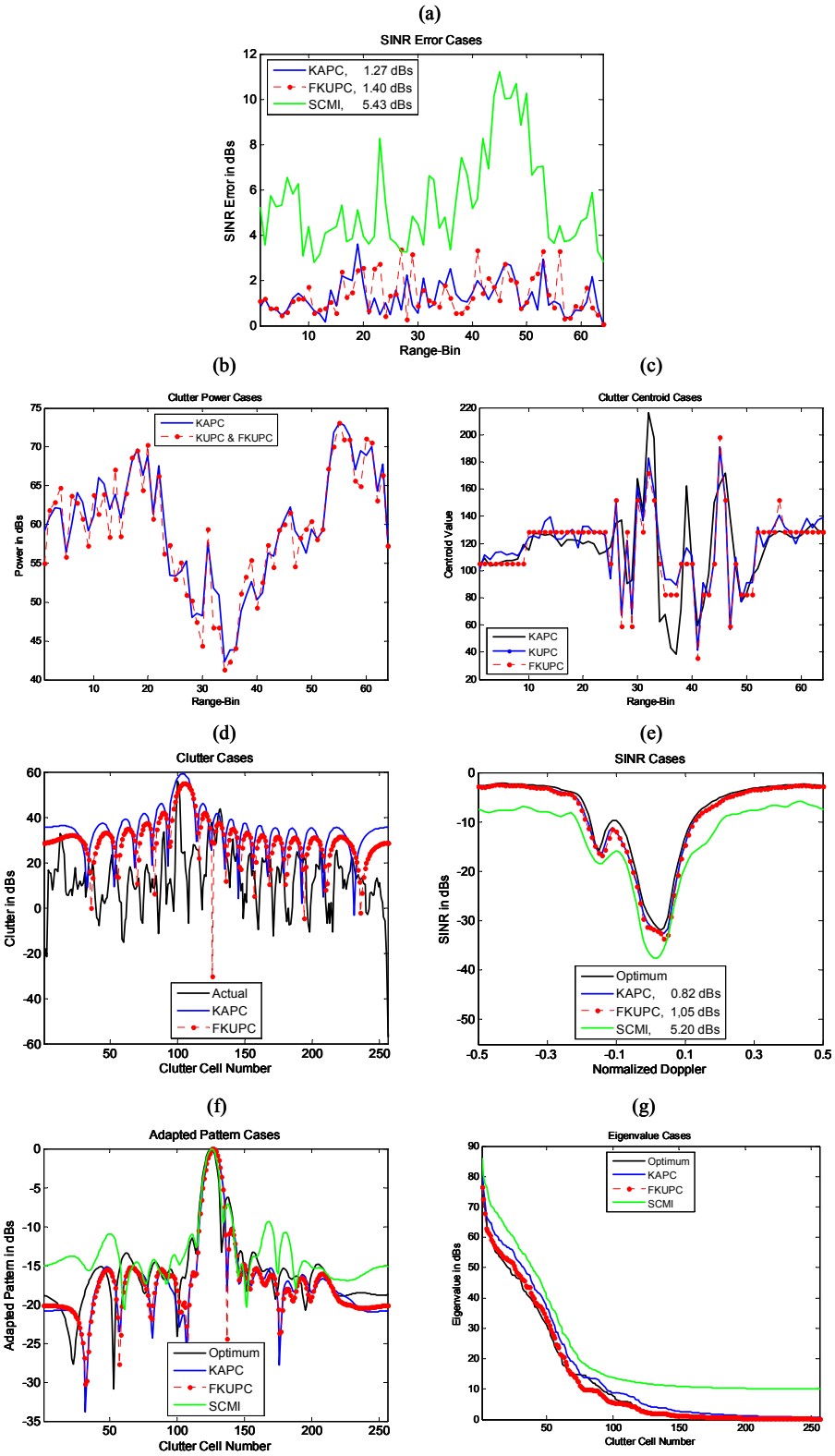

Fig. 6. Eleven (11) CAPs with no Jammers. (a) SINR Error. (b) Range-Bins Powers of Clutter Plus Jammer. (c) Range-Bins Centroids with Clutter Plus Jammer. (d) Range-Bin #1 Clutter and its Predictions. (e) Range-Bin #1 SINRs. (f) Range-Bin #1 Adapted Patterns. (g) Range-Bin #1 Eigenvalues

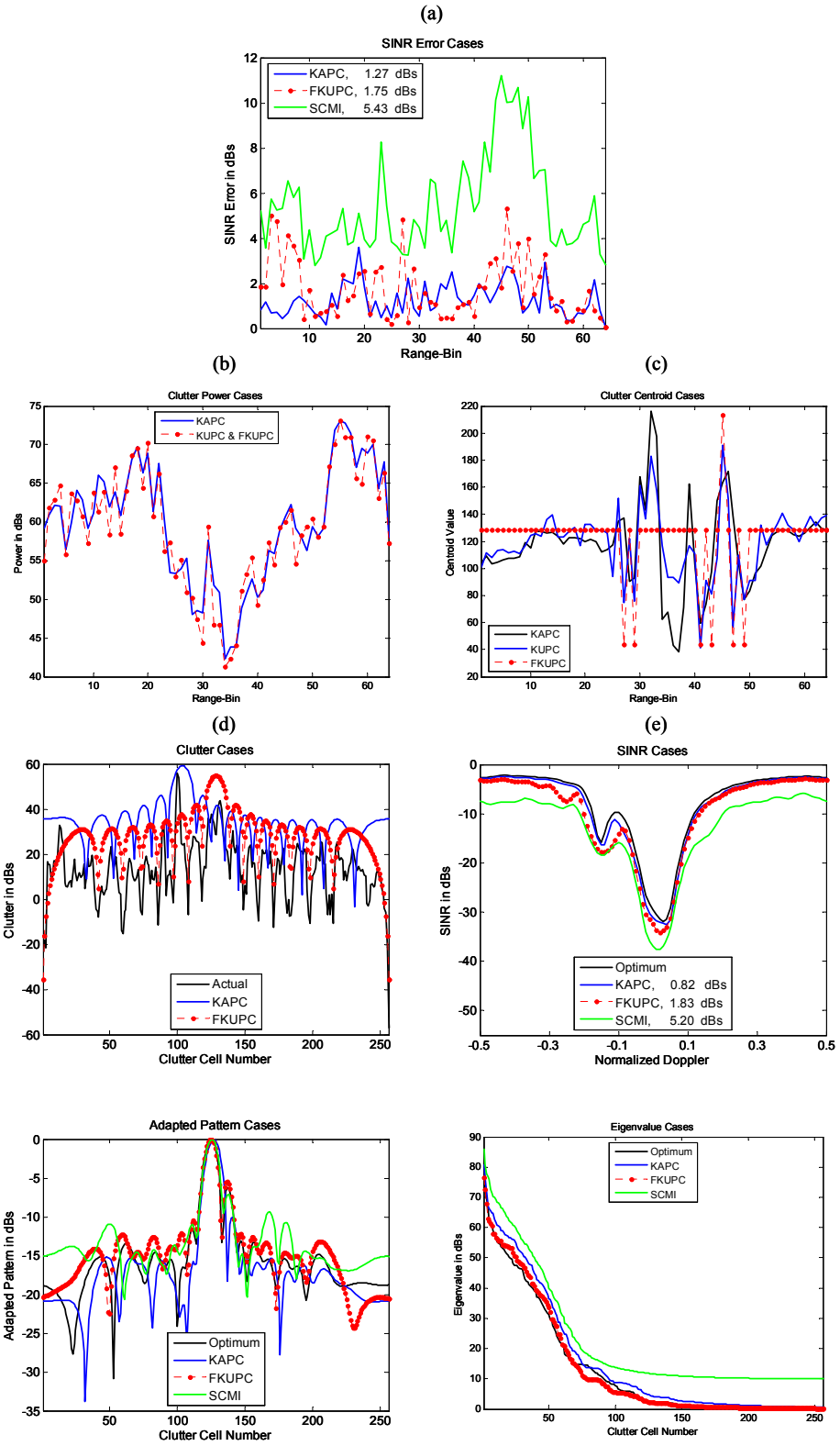

Fig. 7. Three (3) CAPs with no Jammers. (a) SINR Error. (b) Range-Bins Powers of Clutter Plus Jammer. (c) Range-Bins Centroids with Clutter Plus Jammer. (d) Range-Bin #1 Clutter and its Predictions. (e) Range-Bin #1 SINRs. (f) Range-Bin #1 Adapted Patterns. (g) Range-Bin #1 Eigenvalues

Table 1. Radar Simulation Parameters

a.	Antenna	N=16, M=16, d/λ=½, $\sigma_n^2 = 1$ Front antenna gain constant, (1): K^f = 56 dBs Back antenna gain constant : K^b = -40 dBs Carrier frequency, (9): $f_c = 10^9$ Hz Pulse repetition frequency, (10): $f_r = 10^3$ Hz Antenna array misalignment, (13): $\theta_{AAM} = 2^o$
b.	Clutter	$N_c = 256$ Radar's *ratio* β, (19): $\beta = 1$
c.	Jammers	Jammers were used at -60°, -30° and 45° with 52, 55 and 66 JNRs in dBs, respectively, inclusive of antenna gains.
d.	Range Walk	Fraction of remaining area after range walk, (33): ρ=0.999999.
e.	Internal Clutter Motion	Shape factor, (35): $b = 5.7$ Wind-speed, (37): $\omega = 15$ mph
f.	Channel Mismatch: Narrowband	Amplitude error, (50): $\Delta\varepsilon_i = 0$ for all i, Phase-error, (50): $\Delta\gamma_i$ fluctuates with a 5° rms for all i
h.	Channel Mismatch: Finite-Bandwidth	Amplitude peak deviation, (41): $\Delta\varepsilon = 0.001$, Phase peak deviation, (41): $\Delta\phi = 0.1^o$
i.	Channel Mismatch : Angle-Dependent	Bandwidth, (45): $B = 10^8$ Hz Mainbeam width, (45): $\Delta\theta = 28.6^o$

REFERENCES

[1] Guerci, J. R. and Feria, E. H., "Application of a least squares predictive-transform modeling methodology to space-time adaptive array processing," *IEEE Trans. On Signal Processing,* vol. 44, no. 7, pp.1825-1833, July 1996.

[2] Guerci, J. R. and Baranoski, E., " Knowledge-aided adaptive radar at DARPA", *IEEE Signal Processing Magazine*, vol. 23, no. 1, pp. 41-50, January 2006

[3] Feria, E. H., "Latency-information theory: A novel latency theory revealed as time-dual of information theory", *Proceedings of IEEE Signal Processing Society:* DSP Workshop and SPE Workshop, Marco Island, Florida, Jan. 2009

[4] ---------, "A predictive-transform compression architecture and methodology for KASSPER," *Final Technical Report*, DARPA Grant FA8750-04-1-0047, May 2006.

[5] ---------, "Predictive-transform estimation," *IEEE Transaction On Signal Processing*, vol. **39**, no. 11, pp. 2481-2499, Nov. 1991.

[6] ---------, "Matched processors for optimum control", *City University Of New York (CUNY)*, Ph.D. in E.E., Aug. 1981 and Feria, E. H., "Matched processors for quantized control: A practical parallel processing approach," *International Journal of Controls*, Vol. 42, Issue 3, pp. 695-713, Sept. 1985.

[7] Guerci, J. R. " Space-time adaptive processing for radar", *Artech House*, 2003

[8] Web site, http://feria.csi.cuny.edu